JOURNAL OF CATALYSIS 104, 396–412 (1987)

The Effect of Boron on the State and Dispersion of Co/Al_2O_3 Catalysts

MICHAEL A. STRANICK, MARWAN HOUALLA, AND DAVID M. HERCULES

Department of Chemistry, University of Pittsburgh, Pittsburgh, Pennsylvania 15260

Received August 21, 1986; revised October 30, 1986

The influence of boron on the chemical state and dispersion of Co/Al_2O_3 catalysts has been investigated by bulk and surface spectroscopic techniques. Three series of Co/Al_2O_3 catalysts were studied: one containing a constant Co loading of 3 wt% and boron loadings of 0.3 to 3 wt%, and two series containing 0.7 to 10 wt% Co and constant boron loadings of either 0 or 3 wt%. In the absence of boron, Co dispersion decreased with increasing Co loading above 1.5 wt% Co. The presence of boron had little effect on Co dispersion at low Co loadings, while catalysts with Co loadings in excess of 1.5 wt% exhibited an increase in Co dispersion compared to boron-free catalysts. X-ray photoelectron spectroscopy, diffuse reflectance spectroscopy, and gravimetric analysis were used to quantify the Co species present on the catalysts as a function of both Co and boron loading. In the absence of boron, Co exists as tetrahedral and octahedral Co^{2+} at low Co loadings, while Co_3O_4 is the primary phase at higher Co loadings. In the presence of boron, Co_3O_4 formation is suppressed for catalysts with Co loadings less than 8 wt% in favor of octahedral Co^{2+} and minor amounts of Co borate. The formation of Co_3O_4 occurs at Co loadings greater than 6 wt% for boron-containing catalysts. A mechanism is described to account for the effect of boron on the dispersion and chemical state of Co.

INTRODUCTION

Numerous studies have focused on the use of additives to modify interactions between the active phase and carrier of supported metal catalysts. Changes in active phase/support interactions can affect the chemical state and dispersion of the active phase and hence alter catalyst activity. For example, the effect of alkali cations on the state and dispersion of nickel, cobalt, and molybdenum supported on alumina have been reported (*1–5*). Changes in the surface properties of nickel and cobalt oxides supported on Ge^{4+}-, Ga^{3+}-, and Zn^{2+}-modified aluminas have also been described (*6–12*).

The present study concentrates on the influence of boron on the state and dispersion of cobalt supported on γ-alumina. Modification of the acid–base properties of alumina by boron is well known (*13, 14*) and alumina–boria itself has been used as an acidic cracking catalyst (*15*). It has been shown that the hydrogenolysis activity of $Ni–Mo/Al_2O_3$ (*16*) catalysts and the CO hydrogenation activity of Ru/Al_2O_3 catalysts increase as a result of boron support modification (*17*). An increase in the activity of Pt/Al_2O_3 reforming catalysts modified with boron has also been reported (*18*).

Although the influence of boron on catalyst activity has been investigated, few studies have been conducted of the effect of boron on active phase/support interactions. Previous work by one of the authors has shown that an increase in both cobalt dispersion and cobalt surface phase formation occurs as a result of boron addition to the alumina support (*19*). An increase in surface phase formation has also been reported for nickel oxide supported on boron-modified alumina (*20*). Thus, a systematic study of the influence of boron on the state and dispersion of Co/Al_2O_3 catalysts has been conducted using bulk and surface-sensitive techniques, with the primary goal being to identify and quantitate the various metal species present on the catalyst sur-

0021-9517/87 $3.00

face as a function of both boron and cobalt loading.

EXPERIMENTAL

Catalyst Preparation

A series of boron-modified alumina carriers (0.3 to 3 wt% boron) was prepared by pore volume impregnation of γ-alumina (Harshaw Chemical Co., AL-1401P; BET surface area: 180 m^2/g; pore volume: 0.43 ml/g) with solutions containing various amounts of boric acid. Samples containing 2 and 3 wt% boron were prepared by double impregnation of the alumina using one-half the required amount of boron for each impregnation step. Samples were dried at 130°C for 4 h between impregnation steps. All samples in the series were finally dried at 130°C for 16 h then calcined in air for 6 h at 600°C. The BET surface area of the alumina was unchanged (180 $\pm$ 5 m^2/g) as a result of boron impregnation.

Cobalt was deposited on the boron-modified carrier by pore volume impregnation with cobalt nitrate solutions. A series of catalysts (designated C3Bx) was prepared using the boron-modified aluminas and containing a constant cobalt loading of 3 wt% as Co metal. A loading of 3 wt% Co was chosen because it is typical of many commercial HDS catalysts. Two additional catalyst series were prepared with Co contents ranging from 0.7 to 10 wt% Co. One series (designated CyB0) utilized unmodified alumina and the other (designated CyB3) employed a support having a boron loading of 3 wt%. Samples were dried at 130°C and calcined at 600°C. Catalysts were finely ground to minimize the effects of inhomogeneity on surface analytical measurements.

Bulk Characterization Techniques

X-ray diffraction (XRD). X-ray diffraction patterns of catalyst samples were obtained with a Diano 700 diffractometer, which utilizes nickel-filtered Cu$K\alpha$ radiation. Diffraction patterns were obtained with an X-ray gun operated at 50 kV and 25 mA, using a scan rate of 0.4° min^{-1} (2θ). Samples were run as powders mounted on glass slides using silicone grease as an adhesive. Compound identification was accomplished through comparison of measured spectra with ASTM powder diffraction file data.

Laser Raman spectroscopy (LRS). Laser Raman spectra were obtained with a Spex Ramalog spectrometer which utilizes holographic gratings. The excitation source was the 514.5-nm line from a Spectra-Physics argon-ion laser, which delivered approximately 50 mW of power measured at the sample. Reported peaks are accurate to within ± 2 cm^{-1}. Samples were pressed into pellets with a KBr support and rotated off-axis to prevent excessive heating by the laser beam.

Diffuse reflectance spectroscopy (DRS). Diffuse reflectance spectra of Co catalyst powders were obtained using a Beckman Acta MVI spectrophotometer equipped with a Harrick DRA-2CB diffuse reflectance attachment. Spectra were recorded in the 350- to 800-nm range. Quantitation of tetrahedral Co^{2+} was accomplished for samples which contain no Co_3O_4 by employing the Kubelka–Munk treatment (*21*). Absence of Co_3O_4 was determined from XRD, LRS, and gravimetric data. A series of standard $CoAl_2O_4/Al_2O_3$ mixtures was prepared with tetrahedral Co^{2+} contents ranging from 0 to 15 mg Co^{2+}/g Al_2O_3. The Kubelka–Munk function was determined for each standard mixture at 625 nm (the maximum in the Co^{2+} tetrahedral band) and a linear calibration curve of Kubelka–Munk function versus tetrahedral Co^{2+} content was obtained. Comparison of the Kubelka–Munk function at 625 nm of catalyst samples with the calibration curve yielded the tetrahedral Co^{2+} content of the catalysts. The quantity of octahedral Co^{2+} was determined by difference.

Microbalance. Catalyst reduction/oxidation behavior was studied using a Cahn 113 microbalance system. Prior to reduction, oxidic samples were dried at 500°C in ultra-

high purity 10% O_2/He (99.99% O_2, 99.999% He) until a constant weight was achieved. Samples were then reduced in a flow of ultrahigh purity (99.999%) hydrogen at a temperature of 500°C for 12 h, followed by reoxidation at the same temperature in O_2/He. The percentage of Co existing as Co_3O_4 was calculated from the weight change measured during the reduction/reoxidation step relative to the weight change which would be expected assuming all Co was present as Co_3O_4. Thus percentage reduction reflects the percentage of Co_3O_4 in the oxidic catalyst.

Surface Characterization

X-ray photoelectron spectroscopy (ESCA or XPS). X-ray photoelectron spectra of oxidic catalysts were obtained with a Leybold–Heraeus LHS-10 surface analysis system interfaced to a Hewlett–Packard 1000 computer. In the present study, an aluminum anode (Al$K\alpha$ = 1486.6 eV) operated at 12 kV and 20 mA was employed. The residual pressure inside the spectrometer was 10^{-8} Torr or lower. ESCA measurements were done on catalyst powders which had been dusted onto double-sided adhesive tape and mounted on the spectrometer probe.

It has been shown that the intensity ratio of supported phase and carrier ESCA peaks is related to the dispersion of the supported phase (*22–25*). In the present work, the Co/Al intensity ratios predicted for monolayer Co coverage were calculated using the model of Kerkhof and Moulijn (*25*). Cobalt speciation was determined from ESCA analysis of chemically treated catalysts using a method which accounts for differences in the dispersion of the Co phases present on the catalyst surface (*26*).

An AEI ES200 spectrometer was utilized to obtain ESCA spectra of reduced or sulfided catalysts. This permitted transfer of a treated catalyst from an external reaction chamber to the spectrometer without exposure to air, using a sealable probe. The reaction chamber and sealable probe have been described in detail elsewhere (*27, 28*). Samples were mounted on the sealable probe as pellets pressed at 2000 kg/cm^2. Samples were reduced in a flow of ultrahigh purity hydrogen for 12 h at 500°C or sulfided in a flow of 15% H_2S/H_2 for 12 h at 400°C. The AEI instrument was interfaced to an Apple IIe microcomputer and was equipped with an aluminum anode operated at 12 kV and 20 mA. The residual pressure inside the spectrometer was 5×10^{-8} Torr.

ESCA binding energies of catalyst samples were referenced to the Al 2*p* line at 74.5 eV. The Al 2*p* binding energy was previously determined through deposition of gold onto γ-alumina and referencing to the Au $4f_{7/2}$ line at 83.3 eV (*29*). The binding energies of standard compounds were referenced to the C 1*s* line at 284.6 eV, the value measured for catalyst samples. Binding energy values were measured with a precision of ±0.15 eV or better.

Ion scattering spectroscopy (ISS). Ion scattering spectra of catalyst samples were obtained using a 3M Model 525 ion scattering spectrometer which employs a cylindrical mirror analyzer to measure the energy of backscattered ions. An incident ion beam of $^3He^+$ ions with a kinetic energy and current density of 2 keV and 2×10^{-7} A/cm^2, respectively, was employed. This corresponds to an approximate sputtering rate of 3 monolayers/h. The base pressure inside the spectrometer was 1×10^{-8} Torr prior to backfilling the analysis chamber with scattering gas to a pressure of 1×10^{-5} Torr. Samples were pressed into pellets as described above and mounted on the ISS probe for analysis. ISS data which are presented as supported phase/carrier peak intensity ratios are the average of at least four spectra measured after the sample had been exposed to the ion beam for 10 min. The total time that the catalyst was exposed to the ion beam was not greater than 30 min. Intensity ratios from consecutive scans were reproducible to within ±0.06, indicating that there was no significant sputtering of the samples.

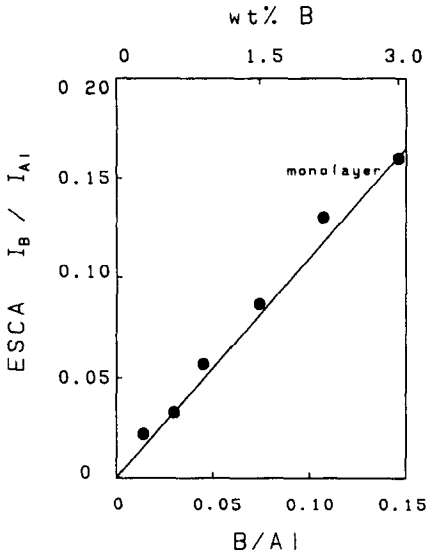

FIG. 1. ESCA B 1*s*/Al 2*s* intensity ratios versus the B/Al atomic ratio for B/Al_2O_3 carriers.

RESULTS

BORON-MODIFIED ALUMINA

Bulk Characterization

XRD. The X-ray diffraction pattern of γ-Al_2O_3 modified with 3 wt% boron exhibited no diffraction lines in addition to those of the alumina, suggesting a well-dispersed boron phase. The intensities of the alumina lines were lower by 25% for the boron-modified carrier compared to the unmodified material.

LRS. The laser Raman spectrum of the boron-modified alumina was similar to that for unmodified alumina (*29*); no bands were observed in the 100- to 1200-cm^{-1} range. The Raman spectra of the reference compound H_3BO_3 was measured and exhibited intense peaks at 880 and 500 cm^{-1}, in agreement with published values (*30*). A Raman spectrum of B_2O_3 could not be obtained due to fluorescence problems; however, bands at 806 and 602 cm^{-1} have been reported (*20*). The absence of bands in the Raman spectrum of the boron-modified alumina indicates that neither H_3BO_3 nor B_2O_3 is present on the alumina. The phase diagram of the Al_2O_3–B_2O_3 system reveals that $9Al_2O_3 \cdot 2B_2O_3$ is the aluminum borate compound which could form at the boron loadings employed in this study (*31*). The Raman spectrum of aluminum borate, $9Al_2O_3 \cdot 2B_2O_3$, exhibited no significant bands in the 100- to 1200-cm^{-1} range.

Surface Characterization

ESCA. The B 1*s* binding energy of the modified aluminas was invariant with boron loading and averaged 192.5 ± 0.1 eV. The B 1*s* binding energies of the reference compounds B_2O_3 and H_3BO_3 have been reported to be 193.5 and 193.2 eV, respectively (*32–34*). Measurements of the B 1*s* binding energies for B_2O_3 and H_3BO_3 in this laboratory were consistent with the literature values. The B 1*s* binding energy of aluminum borate, $9Al_2O_3 \cdot 2B_2O_3$, was 192.5 eV. The B 1*s* binding energies of the modified supports are lower than those of B_2O_3 or H_3BO_3 suggesting that boron is not present as either of these compounds on the support surface. The B 1*s* binding energy of the boron modified carriers is consistent with that of aluminum borate. ESCA binding energy measurements alone, however, are insufficient for determining the presence or absence of specific chemical compounds.

The ESCA B 1*s*/Al 2*s* intensity ratios plotted as a function of the B/Al atomic ratio are shown in Fig. 1 for the boron-modified aluminas. It can be seen that the intensity ratio increases linearly with increasing boron content. Calculated intensity ratios based on the Kerkhof–Moulijn monolayer model are also plotted versus boron content in Fig. 1. There is good agreement between the calculated and experimental intensity ratio values, indicating that boron is well-dispersed on the alumina surface.

COBALT SUPPORTED ON BORON-MODIFIED ALUMINA

Bulk Characterization

XRD. Table 1 indicates the presence (+) or absence (−) of Co_3O_4 for the C3Bx,

TABLE 1

Presence (+) or Absence (−) of Co_3O_4 for C3Bx, CyB0, and CyB3 Catalysts by X-ray Diffraction

wt% B	Co_3O_4		wt% Co	Co_3O_4		
	B/Al atomic ratio	C3Bx		Co/Al atomic ratio	CyB0	CyB3
0	0	+	0.7	0.007	−	−
0.3	0.014	+	1.5	0.013	−	−
0.6	0.029	+	3.0	0.026	+	−
0.9	0.044	+	6.0	0.052	+	−
1.5	0.073	−	8.0	0.069	+	+
2.0	0.11	−	10.0	0.087	+	+
3.0	0.15	−				

CyBO, and CyB3 catalyst series from X-ray diffraction measurements. X-ray diffraction patterns of samples from the C3Bx catalyst series having boron loadings below 1.5 wt% exhibited diffraction lines characteristic of Co_3O_4 in addition to those of the alumina. The intensity of the Co_3O_4 diffraction lines decreased with increasing boron content and no lines except for those of the support were observed for samples containing greater than 1.5 wt% boron. Diffraction patterns of samples from the CyB0 and CyB3 catalyst series containing less than 3 wt% Co were identical to that of the support, indicating the absence of any crystalline Co phases of greater than 4 nm in particle size. The diffraction patterns of CyB0 catalysts having Co loadings in excess of 1.5 wt% exhibited lines characteristic of Co_3O_4. Catalysts containing Co loadings of 1.5 wt% and less exhibited diffraction patterns similar to that of the support. CyB3 catalysts containing Co loadings less than 8 wt% exhibited diffraction patterns similar to that of the support. Co_3O_4 was identified on catalysts containing 8 and 10 wt% Co for both boron-free and boron-modified catalysts.

DRS. Diffuse reflectance spectra of samples from the C3Bx catalyst series are shown in Fig. 2. Samples containing less than 1.5 wt% boron exhibit a broad charge transfer band at 450 nm, characteristic of Co_3O_4 (*35*). A tetrahedral Co^{2+} triplet at 600 nm (*35*) is also visible, superimposed on the broad 700-nm Co_3O_4 band (*35*). At higher boron loadings the Co_3O_4 bands at 450 and 700 nm decrease in intensity, revealing the underlying 600-nm triplet band, due to tetrahedral Co^{2+}, and the 510-nm octahedral Co^{2+} band (*35*). The intensities of both the

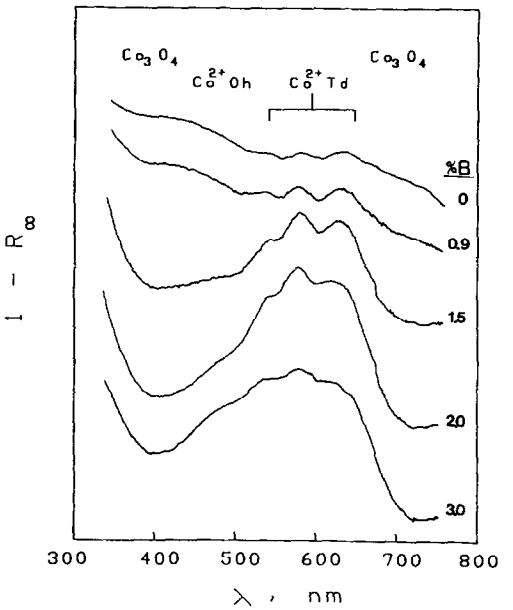

FIG. 2. Diffuse reflectance spectra of C3Bx catalysts shown in order of increasing boron content.

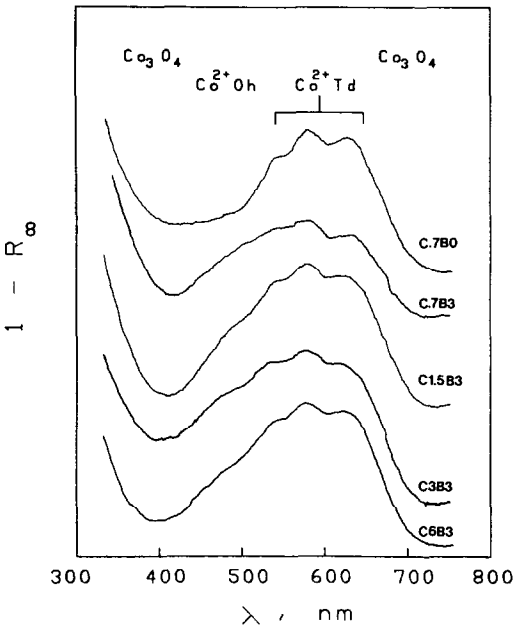

FIG. 3. Diffuse reflectance spectra of Co_3O_4-free CyB0 and CyB3 catalysts shown in order of increasing Co content.

octahedral and tetrahedral Co^{2+} bands increase with increasing boron loading.

DRS spectra of selected catalysts from the CyB0 and CyB3 catalyst series containing less than 8 wt% Co are shown in Fig. 3. Spectra from the CyB3 series all exhibit both the 600-nm tetrahedral Co^{2+} band and the 510-nm octahedral Co^{2+} band. In addition, comparison of the spectra for the C.7B0 and C.7B3 catalysts reveals that the former exhibits only the tetrahedral band, while the latter exhibits both the tetrahedral and octahedral Co^{2+} bands. There was no evidence of Co_3O_4 in any of the above spectra. The DRS spectrum of C1.5B0 was similar to that of C3B0, while spectra of C6B0 and both 8 and 10 wt% Co were similar to that of Co_3O_4.

Table 2 shows the percentages of tetrahedral and octahedral Co^{2+} for Co_3O_4-free catalysts determined from DRS measurements. It can be seen that the presence of boron in the support causes an increase in the percentage of octahedral Co^{2+} at the expense of the tetrahedral species for catalysts containing 0.7 wt% Co. The octahedral Co^{2+} species was the major species in catalysts containing boron at all Co loadings studied. The percentage of tetrahedral Co^{2+} increased from 14 to 29% for the 0.7 and 1.5 wt% Co catalysts, respectively. The tetrahedral Co^{2+} content then decreased with increasing Co loading for the 3 and 6 wt% Co catalysts. A decrease in the percentage of tetrahedral Co^{2+}, from 38 to 22%, was also observed with increasing boron loading for catalysts containing 3 wt% Co.

TABLE 2

Percentage Co^{2+} in Tetrahedral and Octahedral Coordination Determined by Diffuse Reflectance Spectroscopy[a]

Catalyst	% Td	% Oh
C.7B0	79	21
C.7B3	14	86
C.7B3	14	86
C1.5B3	29	71
C3B3	22	78
C6B3	13	87
C3B2	38	62
C3B3	22	78

[a] % Td and % Oh from DRS are ±8% rsd.

LRS. Figure 4 shows the Raman spectra

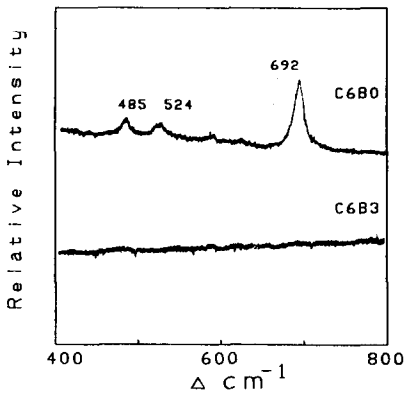

FIG. 4. Laser Raman spectra of C6B0 and C6B3 catalysts.

TABLE 3

Percentage Reduction and Sulfidation of C3Bx Catalysts

Boron loading		% Reduction		% Sulfidation by ESCA[a]
wt%	B/Al atomic ratio	Gravimetric	ESCA[a]	
0	0	55	59	73
0.3	0.014	45	56	65
0.6	0.029	48	54	64
0.9	0.044	48	50	61
1.5	0.073	29	39	59
2.0	0.11	0	0	58
3.0	0.15	0	0	58

[a] Calculated correcting for particle size effects according to Ref. (*26*). Percentages of reduction and sulfidation from ESCA are ±10% rsd.

of calcined catalysts containing 6 wt% Co supported on unmodified and boron-containing carriers. It can be seen that in the absence of boron, Raman bands occur at 692, 524 and 485 cm^{-1}, indicating Co_3O_4 (*36*). The catalyst containing 3 wt% boron (C6B3) exhibited no Raman bands, indicating that boron suppresses the formation of Co_3O_4. The Raman spectra of the calcined 3 wt% Co catalyst containing 3 wt% boron also exhibited no bands, while Co_3O_4 bands were present in the spectra of the boron-free 3 wt% Co catalyst. In addition, Raman analysis of dried 3% Co catalysts did not reveal the presence of Co_3O_4 for either the unmodified or 3% boron-modified catalysts.

Microbalance. Table 3 presents percentage reduction data for C3Bx catalysts, determined gravimetrically. It can be seen that the percentage reduction decreases with increasing boron loading, and above 1.5 wt% boron, no catalyst reduction was observed. Table 4 presents percentage reduction data for the CyB0 and CyB3 catalyst series, based on microbalance measurements. The results of gravimetric studies on the CyB0 series have been discussed elsewhere (*26*). In the absence of

TABLE 4

Percentage Reduction and Sulfidation of CyB0 and CyB3 Catalysts

Co loading		% Reduction				% Sulfidation by ESCA[a]	
wt%	Co/Al atomic ratio	CyB0		CyB3		CyB0	CyB3
		Gravimetric	ESCA[a]	Gravimetric	ESCA[a]		
0.7	0.007	0	0	0	0	25	50
1.5	0.013	17	22	0	0	30	49
3.0	0.026	55	59	0	0	73	57
6.0	0.052	92	83	0	0	89	73
8.0	0.069	92	82	55	62	92	78
10.0	0.087	91	89	77	81	94	89

[a] Calculated correcting for particle size effects according to Ref. (*26*). Percentages of reduction and sulfidation from ESCA are ±10% rsd.

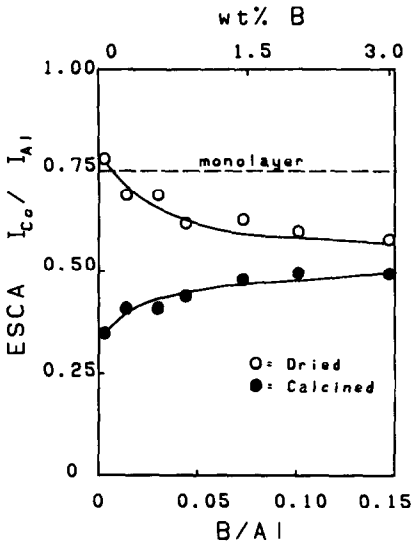

FIG. 5. ESCA Co $2p_{3/2}$/Al 2*s* intensity ratios versus the B/Al atomic ratio for dried and calcined C3Bx catalysts.

boron (CyB0 series), catalyst reduction was observed at all Co loadings in excess of 0.7 wt%. Catalysts from the CyB3 series did not exhibit a weight change during reduction/reoxidation for Co loadings less than 8 wt% Co, indicating the absence of Co_3O_4. The percentage reduction determined for the boron-containing catalysts having 8 and 10 wt% Co were significantly below those of the boron-free samples having similar Co loadings. Thus, gravimetric measurements are in agreement with other bulk characterization techniques with regard to the suppression of Co_3O_4 formation by boron support modification.

SURFACE CHARACTERIZATION: OXIDIC CATALYSTS

C3Bx Series

ESCA. The B 1*s* binding energies of the C3Bx samples were invariant throughout the catalyst series and averaged 192.6 ± 0.1 eV, in good agreement with the B 1*s* binding energy of the modified alumina in the absence of Co. The Co $2p_{3/2}$ binding energies of the catalyst series were unaffected by the presence of boron and averaged 782.2 ± 0.1 eV. The Co $2p_{3/2}$ binding energies of the reference compounds Co_3O_4 and $CoAl_2O_4$ were 780.6 and 782.0 eV, respectively, in agreement with published values (*37*). The measured Co $2p_{3/2}$ binding energy value coupled with the presence of a characteristic shake-up satellite at 786.6 eV in all spectra indicate that a $CoAl_2O_4$-like surface phase exists on the surface of C3Bx catalysts.

Figure 5 shows the Co $2p_{3/2}$/Al 2*s* intensity ratio as a function of the B/Al atomic ratio for dried and calcined C3Bx catalysts. The intensity ratio values for monolayer Co coverage calculated using the Kerkhof–Moulijn model are also indicated. In the case of the dried samples, the Co/Al intensity ratios decrease with increasing boron content. Conversely, the Co/Al intensity ratios of the calcined samples increase with increasing boron loading. In both the dried and calcined series, the change in Co/Al intensity ratio with increasing boron loading is less than 25% relative to the unmodified samples. The Co/Al intensity ratios of the dried catalysts at low boron loadings do not differ significantly from the calculated monolayer value; however, at higher boron

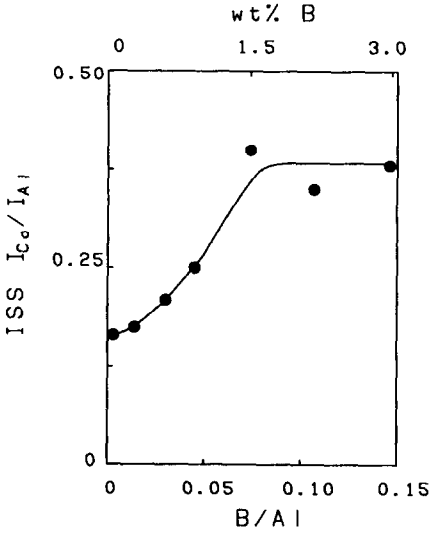

FIG. 6. ISS Co/Al intensity ratios versus the B/Al atomic ratio for calcined C3Bx catalysts.

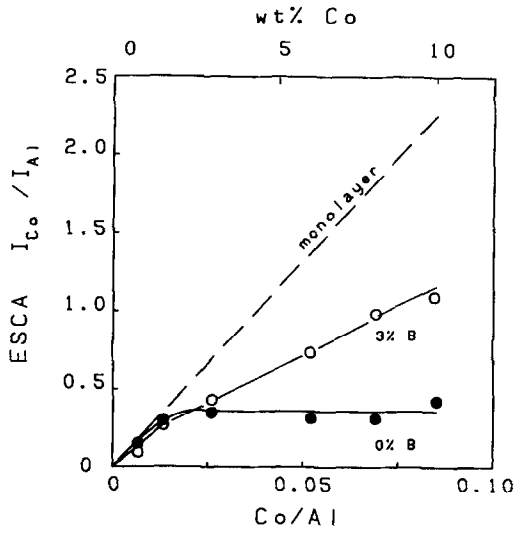

FIG. 7. ESCA Co $2p_{3/2}$/Al 2*s* intensity ratios versus the Co/Al atomic ratio for calcined CyB0 and CyB3 catalysts.

loadings the experimental intensity ratios are below that of the monolayer level. The Co/Al intensity ratios of the calcined samples are significantly lower than the monolayer value at all boron loadings.

ISS. The $^3He^+$ ISS Co/Al intensity ratios plotted as a function of the B/Al atomic ratio for the C3Bx catalyst series are shown in Fig. 6. An increase in the Co/Al intensity ratio with increasing boron content is observed above a B/Al atomic ratio of 0.014 (0.3 wt% B). A constant Co/Al intensity ratio value is attained at loadings above a B/Al atomic ratio of 0.075 (1.5 wt% B). The Co/Al intensity ratio of the catalyst containing a B/Al atomic ratio of 0.15 (3 wt% B) is approximately twice that of the unmodified catalyst.

CyB0 and CyB3 Series

ESCA. The ESCA Co $2p_{3/2}$ binding energies for CyB0 and CyB3 catalysts decreased with increasing Co content. This decrease in binding energy indicates an increase in Co_3O_4 formation with increasing Co loading. A decrease in the Co $2p_{3/2}$ binding energy with increasing Co content has been observed previously for unmodified Co/Al_2O_3 catalysts (*38*). Boron-modified samples containing 1.5 to 8 wt% Co exhibited higher Co $2p_{3/2}$ binding energies than boron-free catalysts. The higher Co binding energy of the modified samples is consistent with less Co_3O_4 formation in the presence of boron. The B 1*s* binding energy did not change significantly with Co loading and averaged 192.5 ± 0.1 eV.

Figure 7 shows the ESCA Co $2p_{3/2}$/Al 2*s* intensity ratios plotted versus the Co/Al atomic ratio for the CyB0 and CyB3 series. Also plotted are the intensity ratios calculated from the Kerkhof–Moulijn model for monolayer Co coverage. The Co/Al intensity ratio data for the CyB0 series have been discussed elsewhere (*26*) and show that the dispersion of Co decreases with increasing Co loading. The Co/Al intensity ratios of samples containing 3 wt% boron are not significantly different from the Co/Al intensity ratios of boron-free samples at low Co loadings. However, at Co/Al atomic ratios greater than 0.013 (1.5 wt%), the Co/Al intensity ratios continue to increase with increasing Co content for the boron-modified catalysts, while those of the unmodified catalysts remain constant. This indicates that addition of boron improves Co dispersion. The Co/Al intensity ratios of the boron-modified catalysts with Co/Al atomic ratios of 0.007 and 0.013 (0.7 and 1.5 wt% Co) were consistent with the intensity ratios predicted for monolayer Co coverage. The CyB3 catalysts having higher Co loadings exhibited intensity ratios below the values predicted by the monolayer model.

ISS. The $^3He^+$ ISS Co/Al intensity ratios plotted as a function of Co content for CyB0 and CyB3 catalysts are shown in Fig. 8. In the absence of boron, the Co/Al intensity ratios remain essentially constant for all Co loadings. The presence of boron had little effect on the Co/Al intensity ratio of the sample having a Co/Al atomic ratio of 0.007 (0.7 wt% Co); however, at higher Co loadings samples containing boron exhibited significantly higher Co/Al intensity ratios.

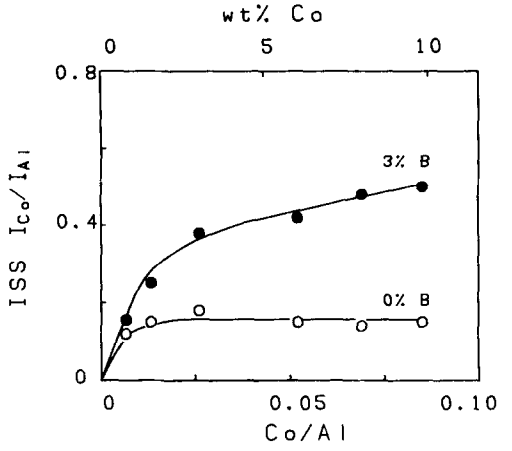

FIG. 8. ISS Co/Al intensity ratios versus the Co/Al atomic ratio for calcined CyB0 and CyB3 catalysts.

SURFACE CHARACTERIZATION: REDUCED AND SULFIDED CATALYSTS

C3Bx Series

ESCA. Table 3 presents the percentage reduction and sulfidation of C3Bx catalysts determined by ESCA, employing the particle size correction described elsewhere (*26*). The percentage of Co reduction for C3Bx catalysts decreased dramatically with increasing boron loading. Samples containing 0 to 1.5 wt% boron exhibited a decrease in percentage reduction from 59 to 39%, while at higher boron contents no Co reduction was observed. The percentage reduction calculated from ESCA data and employing the correction for particle size effects is consistent with gravimetric reduction data. The percentage of Co sulfidation also decreased with increasing boron content from 73% for the boron free sample to 58% for the sample containing 3 wt% boron. The decrease in the percentage sulfidation was much smaller than that observed for reduction; some sulfidation was observed for all C3Bx catalysts.

CyB0 and CyB3 Series

ESCA. Table 4 presents the percentage reduction and sulfidation of CyB0 and CyB3 catalysts determined by ESCA, employing the particle size correction (*26*). Catalysts from both series containing 0.7 wt% Co exhibited no reduction. The percentage reduction of CyB0 catalysts containing 1.5 to 6 wt% Co increased from 22 to 83% with increasing Co loading, while catalysts from the CyB3 series containing 1.5 to 6 wt% Co exhibited no reduction. This indicates that boron suppresses the formation of reducible Co phases for catalysts containing 1.5 to 6 wt% Co. Reduction was observed for catalysts from both series containing 8 and 10 wt% Co; however, the percentage reduction of boron-modified catalysts was less than that for boron-free catalysts. The extent of reduction determined by ESCA was consistent with gravimetric reduction data.

Sulfidation of CyB0 catalysts increased with increasing Co content from 25% for the 0.7 wt% Co sample to 94% for the 10 wt% Co sample. The extent of sulfidation of the boron-modified samples also increased with increasing Co content from 50% for the 0.7 wt% Co catalyst to 89% for the 10 wt% Co catalyst. Below 6 wt% Co the boron-modified samples exhibited a significantly higher degree of sulfidation than the boron-free catalysts. Co loadings of 6 wt% and greater resulted in comparatively lower extents of sulfidation for boron-containing samples. Significant sulfidation was observed for all CyB0 and CyB3 catalysts.

DISCUSSION

BORON-MODIFIED ALUMINA

The bulk characterization of boron-modified alumina presented in this work is consistent with results reported by others (*15*). X-ray diffraction revealed no lines other than those from alumina, indicating the presence of a well-dispersed alumina–boria phase. ESCA data also indicate a high degree of boron dispersion as the measured B/Al intensity ratios are in good agreement with those predicted for monolayer boron coverage. ESCA binding energy data are

inconsistent with the presence of B_2O_3 or H_3BO_3 on the carrier surface. The ESCA B 1*s* binding energies of the modified carriers are consistent with that of aluminum borate, $9Al_2O_3 \cdot 2B_2O_3$, however. The absence of appropriate bands in the Raman spectra also indicate that B_2O_3 and H_3BO_3 are not present on the carrier surfaces. It has been suggested from infrared measurements of alumina–boria catalysts that an Al–O–B bonding arrangement may exist on the catalyst surface (*15*). Reduction in the intensity of the γ-Al_2O_3 X-ray diffraction lines for carriers with high boron loadings indicates disruption of the alumina crystal structure and is consistent with the formation of Al–O–B bonds.

Thus, the data indicate that a strong interaction between alumina and boron exists on the surface of alumina–boria catalysts. X-ray diffraction evidence of a discrete aluminum borate phase such as $9Al_2O_3 \cdot 2B_2O_3$ was not observed in this work or in other published studies of alumina–boria catalysts (*15*). The formation of a highly dispersed, microcrystalline aluminum borate phase or a surface aluminum borate phase could account for the X-ray diffraction and spectroscopic results. A surface aluminum borate phase would not have the long range order necessary for detection by X-ray diffraction but would disrupt the γ-Al_2O_3 crystal structure and decrease the intensity of the alumina diffraction lines. A surface aluminum borate would also exhibit ESCA B 1*s* binding energies similar to those of bulk aluminum borate. In addition, the surface aluminum borate may have a different surface crystal structure than the alumina, since bulk aluminum borate, $9Al_2O_3 \cdot 2B_2O_3$, is orthorhombic (*39*). The defect nature of the support surface must be maintained, however, to allow the accommodation of metal cations.

Effect of Boron on Co Dispersion

C3Bx Series. X-ray diffraction analysis of C3Bx samples revealed a decrease in the intensity of the Co_3O_4 lines with increasing boron loading, suggesting that boron support modification improves Co dispersion. Enhancement of Co dispersion also is indicated by ESCA and ISS Co/Al peak intensity ratios which increase with increasing boron loading for calcined samples. The greater difference in Co/Al intensity ratios from low to high boron loadings in the case of ISS is consistent with the higher surface sensitivity of ISS compared to that of ESCA.

ESCA data published previously showed an increase in the Co/Al intensity ratio with increasing boron loading (*19*). The Co/Al intensity ratios increased to a lesser extent in this work compared to the previously reported data. One explanation for this discrepancy could be that a higher surface area alumina was used in the present study. Another possible reason may lie in slightly different sample preparation conditions. In the present work, Co may be in a more highly dispersed state initially, and thus the effect of boron is less pronounced.

The dispersion of an active phase is often determined by the extent of the interaction between the active phase and the carrier prior to calcination. ESCA Co/Al intensity ratio measurements of dried C3Bx catalysts suggest that Co dispersion decreases with increasing boron loading prior to calcination. This trend in Co/Al intensity ratio was not affected by sample grinding which indicates that changes in catalyst repartition were not significant. At equivalent boron loadings, the Co/Al intensity ratios of calcined C3Bx samples are lower than those for the dried samples, indicating that some decrease in Co dispersion occurs as a result of calcination. At low boron loadings the change in the Co/Al intensity ratio resulting from calcination is greater than the change observed at higher boron loadings, indicating that agglomeration of Co occurs to a lesser extent on boron-modified samples compared to the unmodified carrier.

CyB0 and CyB3 Series. Comparison of the ESCA Co/Al intensity ratios at equivalent Co loadings for the CyB0 and CyB3

series reveals that below 1.5 wt%, Co is well-dispersed on both the modified and unmodified supports. At higher Co loadings, the Co/Al intensity ratios of the boron-containing samples increase with increasing Co loading and are greater than those of the boron-free samples, indicating that boron improves Co dispersion. ISS Co/Al intensity ratio trends for CyB0 and CyB3 catalysts are consistent with those observed by ESCA, further supporting the improvement in Co dispersion by addition of boron. X-ray diffraction results from CyB0 and CyB3 catalysts are also consistent with the ESCA and ISS results. In addition, the effect of boron on Co dispersion depends on Co loading. Boron improves Co dispersion to the greatest extent at high Co loadings where Co dispersion on the unmodified support is poor. Thus, the effect of an additive on the dispersion of a given active phase can be a function of both the active phase and additive loadings.

The Effect of Boron on the Chemical State of Co

Previous work illustrated the use of ESCA for quantitatively determining the species formed on Co/Al_2O_3 catalysts (*26*). It was shown that Co_3O_4 and the Co surface phases (Co^{2+} in octahedral and tetrahedral coordination or cobalt aluminate-like phase) present on oxidic catalysts can be quantified using the ESCA spectra of reduced catalysts, taking into account particle size effects (*26*). The octahedral and tetrahedral components of the surface phase can be determined quantitatively by combining ESCA data from reduced and sulfided catalysts. It has been shown for Co/Al_2O_3 catalysts that octahedrally coordinated Co^{2+}, Co(o), is sulfidable but nonreducible, while tetrahedral Co^{2+}, Co(t), is neither sulfidable nor reducible (*40*). Thus, in the special case where Co_3O_4 is absent, the fractions of Co(o) and Co(t) can be determined directly from the ESCA spectra of sulfided catalysts. Assuming no changes in Co dispersion on sulfidation, the percentage of Co(o) is equivalent to the percentage of sulfided Co, while the percentage of Co(t) is equal to the percentage of unsulfided Co. Using this approach, changes in the speciation of Co resulting from boron support modification can be quantified.

C3Bx Series

Laser Raman and diffuse reflectance spectroscopy indicate that the chemical state of Co supported on the carrier surface changes as a function of boron loading. The disappearance of Co_3O_4 bands in the Raman and DRS spectra of C3Bx catalysts having the highest boron loadings indicates that boron in the support suppresses Co_3O_4 formation. The DRS data also reveal that, as the amount of Co_3O_4 decreases, an increase in the intensities of the tetrahedral and octahedral Co^{2+} bands occurs. An increase in the tetrahedral and octahedral Co^{2+} bands is consistent with an increase in formation of a Co surface phase.

Figure 9 summarizes the percentage distribution of Co species as a function of boron loading calculated using ESCA data from reduced and sulfided catalysts, employing the correction for particle size ef-

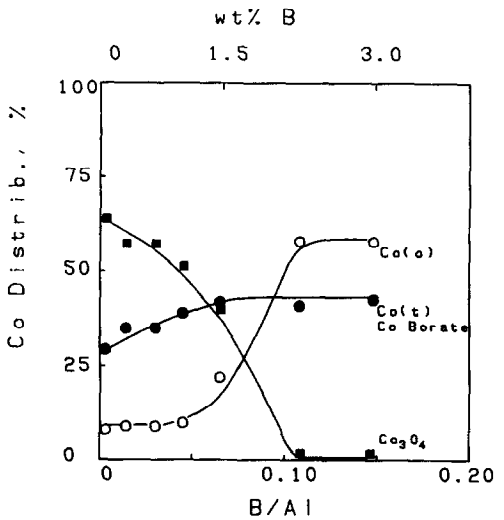

FIG. 9. Distribution of Co species, %, as a function of the B/Al atomic ratio for C3Bx catalysts, determined from ESCA.

fects (*26*). It is evident from Fig. 9 that as the boron loading is increased the amount of Co_3O_4 decreases dramatically with a commensurate increase in the fraction of Co(o). The percentage of Co_3O_4 determined by ESCA for C3Bx catalysts is consistent with that determined gravimetrically, as indicated by the data in Table 3. The percentage of Co(t) increases slightly with increasing boron loading.

In the absence of Co_3O_4, DRS can also be used to quantify the octahedral and tetrahedral components of the surface phase. DRS data (Table 2) are consistent with the ESCA estimation of Co(t) (e.g., the fraction of unsulfided Co, determined from Table 3) for the C3B2 catalyst; 38 and 42% were determined, respectively. DRS and ESCA were not in agreement for the C3B3 catalyst as the Co(t) content from DRS was estimated as 22%, while ESCA indicated 42%. The ESCA determination of Co(t) is an indirect method (i.e., it is assumed that nonreducible, nonsulfidable Co^{2+} is tetrahedrally coordinated), while DRS measures Co(t) directly. Thus, the DRS determination of Co(t) is, in principle, more reliable than by ESCA. The greater Co(t) content determined by ESCA in comparison to DRS for the 3% boron catalyst can be accounted for by the presence of an additional nonreducible, nonsulfidable Co^{2+} species on the catalyst surface. The fact that the discrepancy between ESCA and DRS occurs only at the highest boron loading suggests that this additional Co^{2+} species may be a Co borate phase. The existence of octahedral Co^{2+} borate compounds have been reported in the literature (*41*). The increase in the intensity of the octahedral Co^{2+} band in the DRS spectrum of the 3% boron catalyst may, in part, be due to an octahedral Co^{2+} borate phase. It should be stressed that octahedral Co^{2+} borate is a phase distinct from the octahedral Co^{2+}, Co(o), incorporated into the alumina.

CyB0 and CyB3 Series

It has been shown for CyB0 catalysts that the fraction of Co present as Co_3O_4 increases with increasing Co loading (*26*). The fractions of Co(t) and Co(o) decrease as Co loading increases for CyB0 catalysts (*26*). The major phase present on the surfaces of Co/Al_2O_3 catalysts is Co_3O_4 for CyB0 catalysts having Co loadings in excess of 1.5 wt%. Quantification of Co(t) by DRS for the 0.7 wt% Co catalyst is consistent with that obtained from ESCA analysis of the sulfided catalyst. Both techniques indicate approximately 75% Co(t) on the catalyst surface. The agreement between DRS and ESCA in the determination Co(t) for the 0.7 wt% Co catalyst further confirms that Co(t) is both nonreducible and nonsulfidable.

Laser Raman and diffuse reflectance spectroscopy indicate that formation of Co_3O_4 is suppressed in favor of Co surface phases for CyB3 catalysts containing less than 8 wt% Co. The formation of Co_3O_4 occurs for CyB3 catalysts at loadings of 8 wt% and greater. As in the case of the C3B3 catalyst, DRS and ESCA were not consistent in the determination of Co(t) for Co_3O_4-free CyB3 catalysts. The discrepancy between DRS and ESCA in the determination of Co(t) for Co_3O_4-free CyB3 catalysts is illustrated in Fig. 10. ESCA results indi-

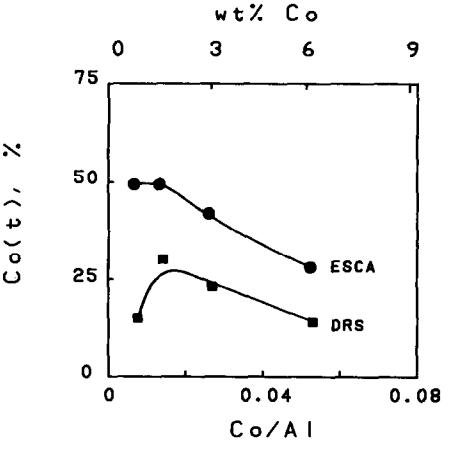

FIG. 10. Percentage of tetrahedral Co^{2+} versus the Co/Al atomic ratio for Co_3O_4-free catalysts determined by DRS and ESCA.

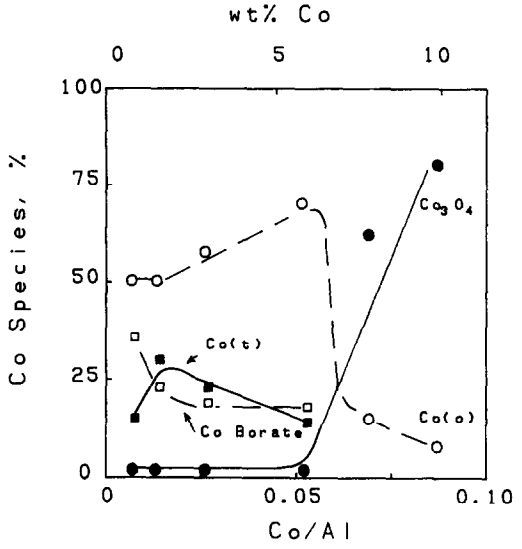

FIG. 11. Percentages of octahedral Co^{2+}, tetrahedral Co_{2+}, and Co borate as a function of the Co/Al atomic ratio from combining DRS and ESCA data, for Co_3O_4-free CyB3 catalysts.

cated a greater fraction of the surface was comprised of Co(t) compared to the DRS data. The discrepancy between DRS and ESCA can again be accounted for by the presence of a nonreducible, nonsulfidable Co borate phase on the CyB3 catalyst surfaces.

By combining ESCA and DRS, the amounts of Co(t) and Co borate can be quantified for the Co_3O_4-free CyB3 catalysts. The percentage of Co borate can be determined by the difference between the percentages of unsulfided Co from ESCA and Co(t) determined by DRS:

$$[\text{Co borate}] = [\text{Co unsulf}]_{\text{ESCA}} - [\text{Co(t)}]_{\text{DRS}}.$$

The percentages of Co(t) and Co borate determined by the combined use of DRS and ESCA are shown in Fig. 11 for Co_3O_4-free CyB3 catalysts. Also shown are the percentages of Co(o) and Co_3O_4, determined from ESCA as described previously (*26*), for all Co loadings studied. The percentage of Co(t) reaches a maximum value of 30% at a Co/Al atomic ratio of 0.013 (1.5 wt% Co), while the percentage of Co borate decreases with increasing Co loading from 36 to 18%. It should be stressed that combining ESCA and DRS to determine Co borate content is only valid if the Co borate phase is assumed to be atomically dispersed. The percentage of Co(o) initially increases with increasing Co loading, attaining a maximum value of 72% at the Co/Al atomic ratio of 0.052 (6 wt% Co). The percentage of Co(o) decreases dramatically at higher Co loadings. Co_3O_4 is absent on the catalyst for Co/Al atomic ratios of 0.052 (6 wt% Co) and lower, with the percentage of Co_3O_4 increasing sharply at higher Co loadings.

The effect of boron on the amount of Co_3O_4 present on Co/Al_2O_3 catalysts determined from ESCA data is illustrated in Fig. 12. In the absence of boron, Co_3O_4 formation occurs at a Co/Al atomic ratio of 0.007 (0.7 wt% Co), with the amount of Co_3O_4 increasing with increasing Co loading. The presence of boron in the support suppresses the formation of Co_3O_4 for catalysts containing less than a Co/Al atomic ratio of 0.069 (8 wt% Co). Formation of Co_3O_4 is observed at Co/Al atomic ratios of 0.069 and 0.087 (8 and 10 wt% Co) for boron-

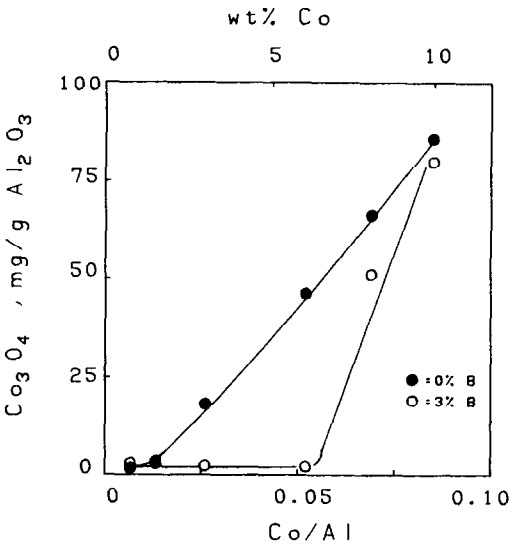

FIG. 12. Co_3O_4 content, in mg/g Al_2O_3, versus the Co/Al atomic ratio for CyB0 and CyB3 catalysts.

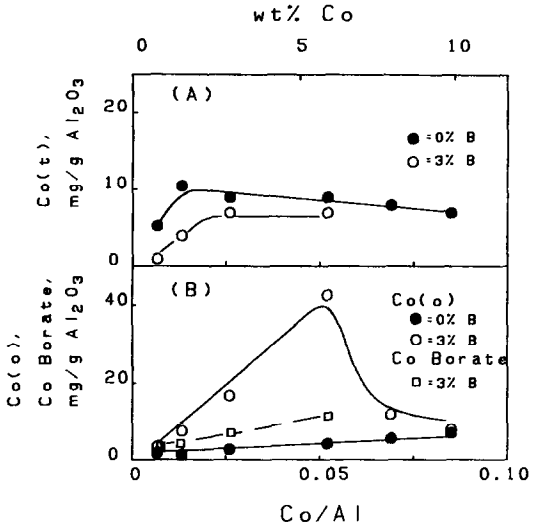

FIG. 13. (A) Tetrahedral Co^{2+} content, in mg/g Al_2O_3, versus the Co/Al atomic ratio for CyB0 and CyB3 catalysts. (B) Octahedral Co^{2+} content, in mg/g Al_2O_3, versus Co/Al atomic ratio for CyB0 and CyB3 catalysts.

containing catalyst, although the amount of Co_3O_4 formed is less than that for the boron-free catalysts by 25 and 10%, respectively.

The effect of boron on the Co(t) content of Co/Al_2O_3 catalysts, determined from DRS and ESCA measurements, is shown in Fig. 13A. It should be noted that an accurate amount of Co(t) cannot be determined for CyB3 catalysts containing greater than 6 wt% Co, as quantification by DRS is hindered by the presence of Co_3O_4. The amount of Co(t) on boron-free Co/Al_2O_3 catalysts initially increases with increasing boron loading and reaches a maximum value at a Co/Al atomic ratio of 0.013 (1.5 wt% Co). A small decrease in Co(t) content is then observed. In the presence of boron, the Co(t) content increases with increasing Co loading and reaches a constant value at approximately a Co/Al atomic ratio of 0.026 (3 wt% Co). The amount of Co(t) is lower for boron-containing catalysts than that for boron-free catalysts.

The influence of boron on the Co(o) content of Co/Al_2O_3 catalysts determined from DRS and ESCA data is illustrated in Fig. 13B. Boron-free catalysts exhibit very low Co(o) contents relative to Co(t) at low Co loadings. The amount of Co(o) increases with increasing Co loading for boron-free catalysts and reaches values comparable to those of Co(t) at high Co loadings. Boron-containing catalysts exhibit a dramatic increase in Co(o) content with increasing Co loading below a Co/Al atomic ratio of 0.069 (8 wt% Co). The amount of Co(o) in boron-containing catalysts increases by as much as a factor of 10 compared to the boron-free catalysts. This increase in Co(o) content occurs at Co loadings where Co_3O_4 is absent on the catalyst. Thus, the formation of Co(o) is favored over Co_3O_4 for boron-containing catalysts having Co loadings below 8 wt%. The amount of Co(o) decreases sharply for catalysts containing Co/Al atomic ratios of 0.069 and 0.087 (8 and 10 wt% Co). This corresponds to the increase in Co_3O_4 formation shown in Fig. 12. Thus at high Co loadings, Co_3O_4 formation is favored over Co(o). The amount of Co borate formed on boron-containing catalysts increases with increasing Co content. For catalysts containing Co/Al atomic ratios of 0.026 and 0.052 (3 and 6 wt% Co), the amount of Co borate which forms is comparable to the amounts of Co(t) and is small relative to the amounts of Co(o).

MECHANISTIC ASPECTS OF Co/Al_2O_3–B CATALYSTS

To rationalize the effect of boron on Co/Al_2O_3 catalysts from a mechanistic standpoint, two related phenomena must be considered: first, the effect of boron on the Co/support interactions which occur during impregnation and second, the effect of boron on the diffusion of Co^{2+} ions into the alumina surface layer during calcination.

Information related to the Co/support interactions which occur during impregnation can be obtained from studying dried catalysts (Fig. 5). Assuming no significant changes in catalyst repartition, the ESCA results indicate that the dispersion of Co

decreases with increasing boron loading for dried C3Bx catalysts. This decrease in dispersion is not due to the formation of Co_3O_4 particles, as evidenced by laser Raman results for the dried catalysts. The decrease in Co dispersion may be due to exposed boron atoms acting as nucleation sites for Co^{2+} precipitation. As the boron loading is increased there is an increase in the number of exposed boron atoms and hence, more nucleation sites for Co aggregates. A decrease in Co dispersion resulting from the precipitation of Co^{2+} around exposed surface boron atoms is reasonable, assuming that the number of nucleation sites is much less than the number of Co^{2+} ions which can precipitate on the support surface. Since the B^{3+} ion is relatively small in size, diffusion of a majority of B^{3+} ions into the support surface layer probably occurs. Thus, a small fraction of boron atoms are exposed at the support surface and can act as nucleation sites for Co^{2+} precipitation.

The chemical state and dispersion of Co in calcined catalysts is determined by the strength of the interaction between Co and the support. In the absence of boron or at low boron loadings, the interaction between the deposited Co and the support surface is weak, relative to that at high boron loadings. Thus, diffusion of Co occurs mainly across the support surface during calcination, resulting in the formation of poorly dispersed Co_3O_4. At high boron loadings, the interaction between the precipitated Co and the modified support surface is stronger than the Co/support interaction for catalysts with low boron loadings. Consequently, Co_3O_4 formation is suppressed and Co diffuses into the alumina surface layer, resulting in the presence of Co^{2+} in primarily octahedral and tetrahedral sites of the alumina lattice. Results from the C3Bx catalyst series are consistent with this mechanism. Calcination of the C3Bx catalysts resulted in a greater decrease in Co dispersion for catalysts having low boron loadings compared to the high boron content catalysts. The increase in dispersion and suppression of Co_3O_4 formation for CyB3 catalysts relative to CyB0 catalysts, in the 1.5 to 6 wt% Co range, further supports this mechanism. The aggregation and stabilization of Co^{2+} ions around surface boron centers also accounts for the formation of small amounts of Co borate. Formation of Co_3O_4 was observed for boron-modified catalysts containing 8 and 10 wt% Co. At these higher Co loadings Co_3O_4 formation is favored via two processes. First, an increase in the concentration of the cobalt nitrate solution would lead to the nucleation and growth of Co_3O_4 precursor at the early stages of impregnation. Second, an insufficient number of exposed surface boron atoms exist to stabilize the precipitated Co^{2+} ions, resulting in a weaker Co/support interaction relative to the lower Co loading catalysts. Thus Co_3O_4 formation occurs in preference to Co surface phase at these loadings.

Octahedral Co^{2+} is the primary Co species found for catalysts having high boron loadings and less than 8 wt% Co. The presence of Co^{2+} in predominantly octahedral coordination can be rationalized by considering the diffusion of boron and Co^{2+} into the alumina surface layer. The diffusion pathways for Co^{2+} ions are influenced by the symmetry of boron ions in the alumina surface layer. There is no direct evidence for the symmetry of boron ions in the alumina surface layer; however, based on the chemistry of boron compounds, a tetrahedral site preference is a logical choice. Thus, if boron occupies vacant tetrahedral sites in the alumina lattice, there is a greater fraction of octahedral sites available to Co^{2+} ions, relative to the fraction of available tetrahedral sites. It is well known that Co^{2+} ions have a strong tetrahedral site preference; however, diffusion into tetrahedral sites is hindered by the occupation of the tetrahedral sites by boron. This general site-blocking model could account for the large amounts of Co^{2+} in octahedral coordination for boron-modified catalysts. The site-blocking model, however, assumes

that the crystal structure of the alumina surface layer is unchanged by the presence of boron. An alternate explanation for the predominance of octahedral Co^{2+} may be proposed if the support surface is comprised of an orthorhombic surface aluminum borate. A different support surface crystal structure may influence the site preference of Co^{2+} ions such that octahedral coordination is favored instead of the tetrahedral coordination found for Co^{2+} in spinellike supports.

ACKNOWLEDGMENTS

The authors acknowledge financial support for this work from the United States Department of Energy, Grant DE-AC02-79ER10485. M.A.S. also acknowledges SOHIO for a graduate fellowship.

REFERENCES

1. Lycourghiotis, A., Defosse, C., Delannay, F., Lemaitre, J., and Delmon, B., *J. Chem. Soc. Faraday I* **76,** 1677 (1980).
2. Houalla, M., Lemaitre, J., and Delmon, B., *J. Chem. Soc. Faraday I* **78,** 1389 (1982).
3. Houalla, M., Delannay, F., and Delmon, B., *J. Phys. Chem.* **85,** 1704 (1981).
4. Kordulis, C., Voliotis, S., Lycourghiotis, A., Vattis, D., and Delmon, B., *Appl. Catal.* **11,** 179 (1984).
5. Lycourghiotis, A., Vattis, D., and Aroni, P., *Z. Phys. Chem.* **120,** 211 (1980).
6. Cimino, A., Lo Jacono, M., and Schiavello, M., *J. Phys. Chem.* **79,** 243 (1975).
7. Lo Jacono, M., Schiavello, M., DeBeer, V. H. J., and Minelli, G., *J. Phys. Chem.* **81,** 1583 (1977).
8. Muralidhar, G., Massoth, F. E., and Shabtai, J., *J. Catal.* **85,** 44 (1984).
9. Massoth, F. E., Muralidhar, G., and Shabtai, J., *J. Catal.* **85,** 53 (1984).
10. Lopez, F., Medina, H., Martinez, N., and Mitchell, P. C. H., *React. Kinet. Catal. Lett.* **22,** 253 (1983).
11. Chin, R. L., and Hercules, D. M., *J. Catal.* **74,** 121 (1982).
12. Fierro, J., Agudo, A., Grange, P., and Delmon, B., *in* "Proceedings, 8th International Congress on Catalysis, Berlin, 1984," Vol. II, p. 363.
13. Benesi, H., *J. Amer. Chem. Soc.* **78,** 5490 (1956).
14. Tanabe, K., "Solid Acids and Bases." Academic Press, New York, 1970.
15. Izumi, Y., and Shiba, T., *J. Chem. Soc. Japan* **37,** 1797 (1964).
16. Lafitau, H., Neel, E., and Clement, J. C., *in* "Preparation of Catalysts" (B. Delmon, P. Jacobs, and G. Poncelet, Eds.), p. 393. Elsevier, Amsterdam, 1976.
17. Okuhara, T., Tamura, H., and Misono, M., *J. Catal.* **95,** 41 (1985).
18. Nadirov, N. K., Vozdvizhenshii, V. F., Kondratkova, N. I., and Fatulina, A. A., *React. Kinet. Catal. Lett.* **27,** 191 (1985).
19. Houalla, M., and Delmon, B., *Appl. Catal.* **1,** 285 (1981).
20. Vorobev, V., Agzamkhodzhaeva, A., Mikita, V., and Abidova, M., *Kinet. Katal.* **25,** 154 (1984).
21. Stone, F. S., *in* "Surface Properties and Catalysis by Non-metals" (J. P. Bonnelle, B. Delmon, and E. Derouane, Eds.), NATO ASI series, p. 237, Reidel, Dordrecht, 1982.
22. Angevine, P. J., Vartuli, J. L., and Delgass, W. N., *in* "Proceedings, 6th International Congress on Catalysis, London, 1976" (G. C. Bond, P. B. Wells, and F. C. Tompkins, Eds.), Vol. 2, p. 611. Chem. Soc. London, 1976.
23. Defosse, C., Canesson, P., Rouxhet, P., and Delmon, B., *J. Catal.* **51,** 269 (1978).
24. Fung, S. C., *J. Catal.* **58,** 454 (1979).
25. Kerkhof, F. P. J. M., and Moulijn, J. A., *J. Phys. Chem.* **83,** 1612 (1979).
26. Stranick, M. A., Houalla, M., and Hercules, D. M., *J. Catal.* **103,** 151 (1987).
27. Patterson, T. A., Carver, J. C., Leyden, D. E., and Hercules, D. M., *J. Phys. Chem.* **80,** 1900 (1976).
28. Ng, K. T., and Hercules, D. M., *J. Phys. Chem.* **80,** 2094 (1976).
29. Zingg, D. S., Makovsky, L. E., Tischer, R. E., Brown, F. R., and Hercules, D. M., *J. Phys. Chem.* **84,** 2898 (1980).
30. Hibben, J., "The Raman Effect and Its Chemical Applications," p. 431. Reinhold, New York, 1939.
31. Gielisse, P. J. M., and Foster, W. R., *Nature (London)* **195,** 69 (1962).
32. Joyner, D. J., and Hercules, D. M., *J. Chem. Phys.* **72,** 1095 (1980).
33. Hendrickson, D. N., Hollander, J. M., and Jolly, W. L., *Inorg. Chem.* **9,** 612 (1970).
34. Nefedov, V. I., Gati, D., Dzhurinskii, B. F., Segurshin, N. P., and Salyn', Ya. V., *Russ. J. Inorg. Chem.* **20,** 1279 (1975).
35. Lo Jacono, M., Cimino, A., and Schuit, G. C. A., *Gazz. Chim. Ital.* **103,** 1281 (1973).
36. Jeziorowski, J., Knozinger, H., Grange, P., and Gajardo, P., *J. Phys. Chem.* **84,** 1825 (1980).
37. Chin, R. L., and Hercules, D. M., *J. Phys. Chem.* **86,** 3079 (1982).
38. Chin, R. L., and Hercules, D. M., *J. Phys. Chem.* **86,** 360 (1982).
39. Scholze, H., *Z. Anorg. Alleg. Chem.* **284,** 272 (1956).
40. Chung, K. S., and Massoth, F. E., *J. Catal.* **64,** 332 (1980).
41. Berger, S. V., *Acta Chem. Scand.* **4,** 1054 (1950).